Electronic Supplementary Material (ESI) for Catalysis Science & Technology.

Supporting Information

Reversion of Catalyst Valence States for Highly Efficient Water Oxidation

Experiment Section

Fabrication of Ni/CC: First, the electrolyte solution was prepared by dissolving 0.15 M of $NiSO_4$ in a solution that contained 0.6 M of H_3BO_3. Then, a two-electrode cell setup was employed with a carbon cloth as the working electrode, and a graphite paper as the counter electrode. Before electrodeposition, the carbon cloth was sintered at 300 °C for 10 min under air atmosphere to improve its hydrophily. A current density of -10 mA cm^{-2} was applied on the working electrode for 1 hour to obtain the Ni/carbon cloth (Ni/CC) electrode.

Fabrication of the SVT catalyst and the activated Ni: A two-electrode cell setup was employed with Ni/CC as the working electrode, and a graphite paper as the counter electrode. 1 M KOH was dissolved into saturated sodium chloride solution, which was served as electrolyte. A current density of 30 mA cm^{-2} was applied on the working electrode for 3 hours to obtain the SVT catalyst (see Figure S1). For the preparation of the activated Ni, 1 M KOH was served as electrolyte and 30 mA cm^{-2} was applied on the working electrode for 3 hours (see Figure S4).

Characterization: Operando XANES was carried out at Singapore Synchrotron Light Source, XAFCA beamline.[1] SEM was performed on ZEISS SEM Supra 40. XPS analysis was carried on an Axis ultra DLD X-ray photoelectron spectrophotometer. All XPS spectra were corrected using the C 1s line at 284.6 eV. The bubble movement process was recorded with the assistance of iX cameras i-speed 726.

Electrochemical measurements: The electrocatalytic experiments were performed in 1 M KOH electrolyte using a VMP3 electrochemical workstation (Bio-logic Inc.). The electrochemical measurements of CV, LSV and chronoamperometry were conducted in a typical three-electrode setup using as-prepared catalytic electrode as the working electrode, a graphite plate as the counter

electrode, and a Hg/HgO (1 M KOH) as the reference electrode. All the potentials were calibrated with respect to a reversible hydrogen electrode (RHE).

The Differential Electrochemical Mass Spectrometry (DEMS) experiment was conducted to qualitative analysis of the amount of O_2 and H_2 evolution during H_2O splitting. A home-made air-tight H-type electrolytic cell was used, in which the working electrode chamber and counter electrode chamber are separated by an anion-exchange membrane (FUMATECH BWT GmbH). The working electrode and counter electrode are SVT catalyst and graphite plate, respectively. 1 M KOH served as the electrolyte.

This H-type electrolytic cell was linked to the DEMS system described in detail in our previous published papers.[2,3] In brief, it is based on a commercial quadrupole mass spectrometer (Hiden HPR-20) with a turbo molecular pump (Pfeiffer Vacuum) that is backed by a dry scroll pump (Edwards) and leak inlet which samples from the purge gas stream. During electrochemical splitting of H_2O, high-purity argon, which acted as the internal tracer gas with a known constant flux, was used as the carrier gas for the purpose of quantifying O_2 and H_2 evolution. The flow rate of purge gas was typically 1.5 mL min^{-1}.

The average potential (E_a) and average overpotential (E_o) of oxygen evolution reaction was calculated using the following formula,

$$E_a = \frac{\int_{t_1}^{t_2} E \cdot t \cdot dt}{t_2 - t_1} \text{ (V)}$$

$$E_o = E_a - 1.23 \text{ (V)}$$

Where E (V vs. RHE) is the recorded potential, t (s) is the time.

We used two-electrode electrolytic cell with an anion-exchange membrane (FUMATECH BWT GmbH) to collect the gas generated during the electrolytic process. The Faradaic efficiency (FE) of O_2 generation was calculated by the equation below,

$$FE_{O_2} = \frac{4 \times 1.01 \times 10^5 (Pa) \times V(L) \times 96485 (C/mol)}{8.314 (J/mol \cdot K) \times T(K) \times Q(C)} (\%)$$

where V (L) is volume of O_2 generation during oxygen evolution reaction, T (K) is room temperature, Q (C) is total amount of charge.

***DFT Calculations*:** Structure optimization and reaction energetics were calculated using density-functional theory (DFT) based Quantum Espresso package with ultrasoft pseudopotentials.[4,5] The exchange-correlation interaction was approximated by the revised Perdew–Burke–Ernzerhof (RPBE) functional.[6] The kinetic energy cutoff for plane wave expansion was set to 50 Ry. To improve the description of localized Ni *d*-electrons in β-NiOOH and β-$Ni(OH)_2$, a simplified rotationally invariant implementation[7] of Hubbard-U model was employed with a value of U=6.6 eV for Ni as reported by Friebel *et al*.[8] The Brillouin zone was sampled using $13 \times 13 \times 3$ Monkhorst-Pack *k*-point grids and a Fermi-level smearing width of 0.1 eV was employed. Spin-polarized calculations were performed on the Ni systems and all structures were optimized until force components below 0.05 eV/Å. The energies of molecules O_2 and H_2O were also calculated as the gas-phase reference. The reaction free energy was calculated as $\Delta G = \Delta E_{DFT} + \Delta ZPE - T\Delta S$, where ΔE_{DFT} is the change in total energy calculated by DFT, and ΔZPE and $T\Delta S$ is the zero-point energy and entropy corrections for the gas-phase molecules taken from reference, respectively.[9]

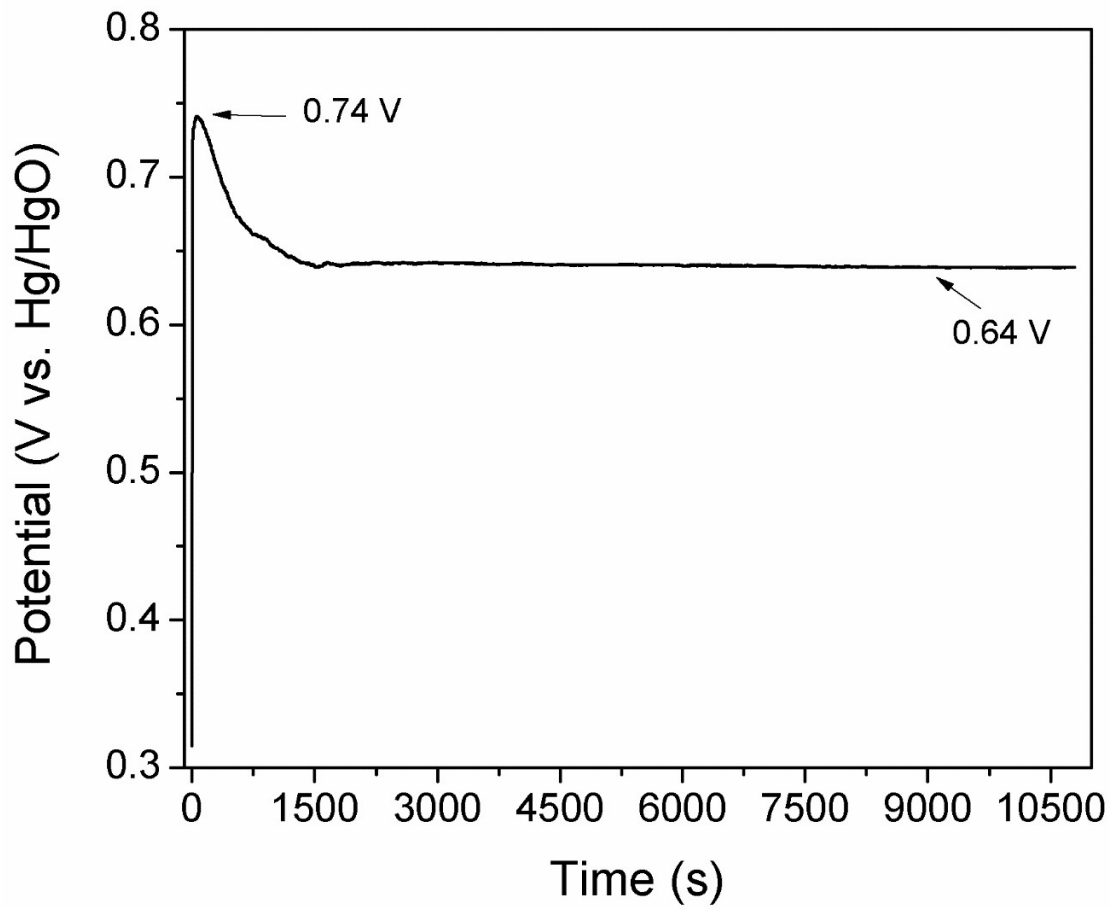

Figure S1**.** Potential of Ni in saturated NaCl and 1 M KOH electrolyte recorded over a long period at a current density 30 mA cm^{-2}.

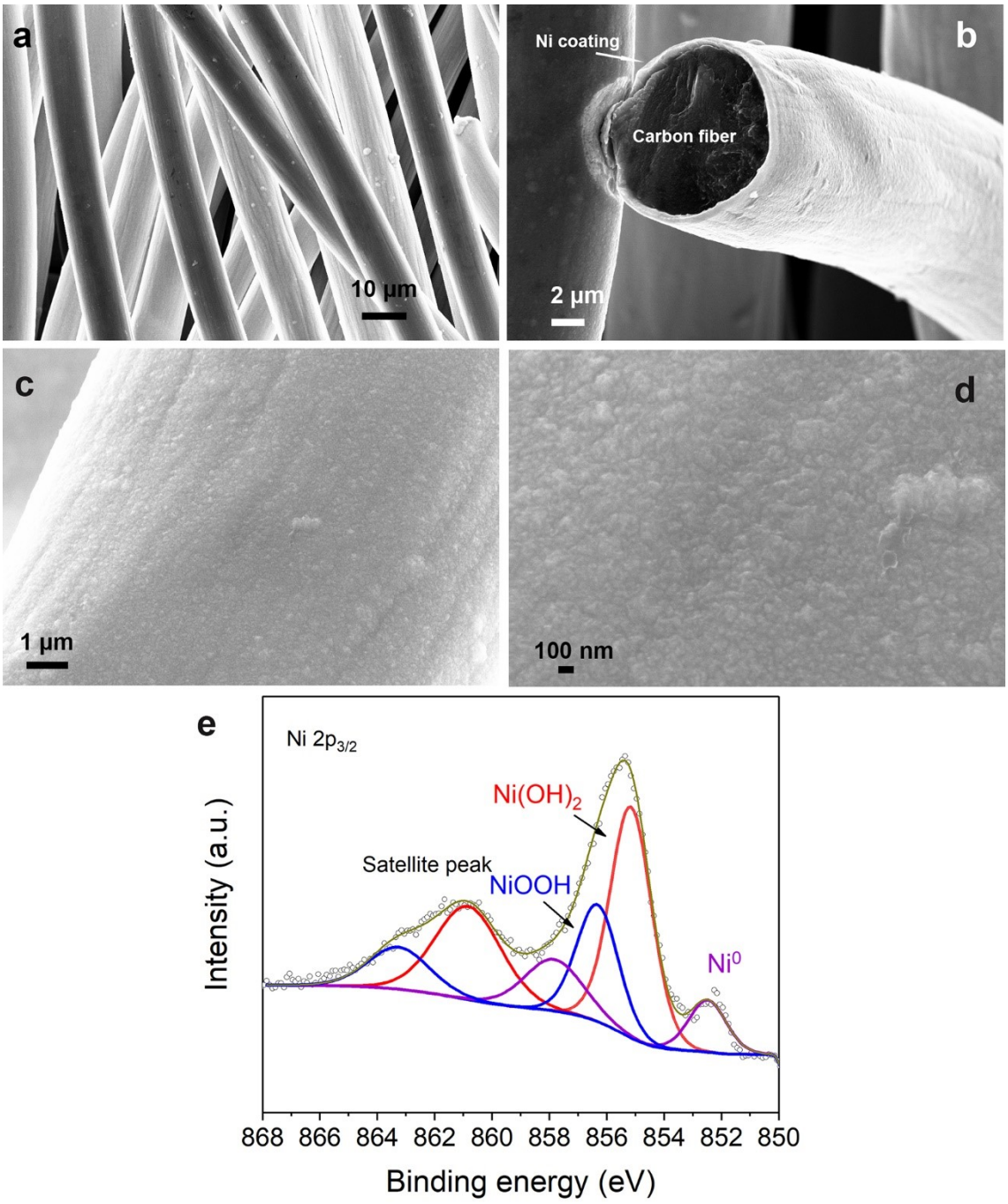

Figure S2**.** The characterization of electrodeposited Ni. a)-d) SEM images of electrodeposited Ni on carbon cloth. e)**,** Ni $2p_{3/2}$ XPS spectra of the electrodeposited Ni.

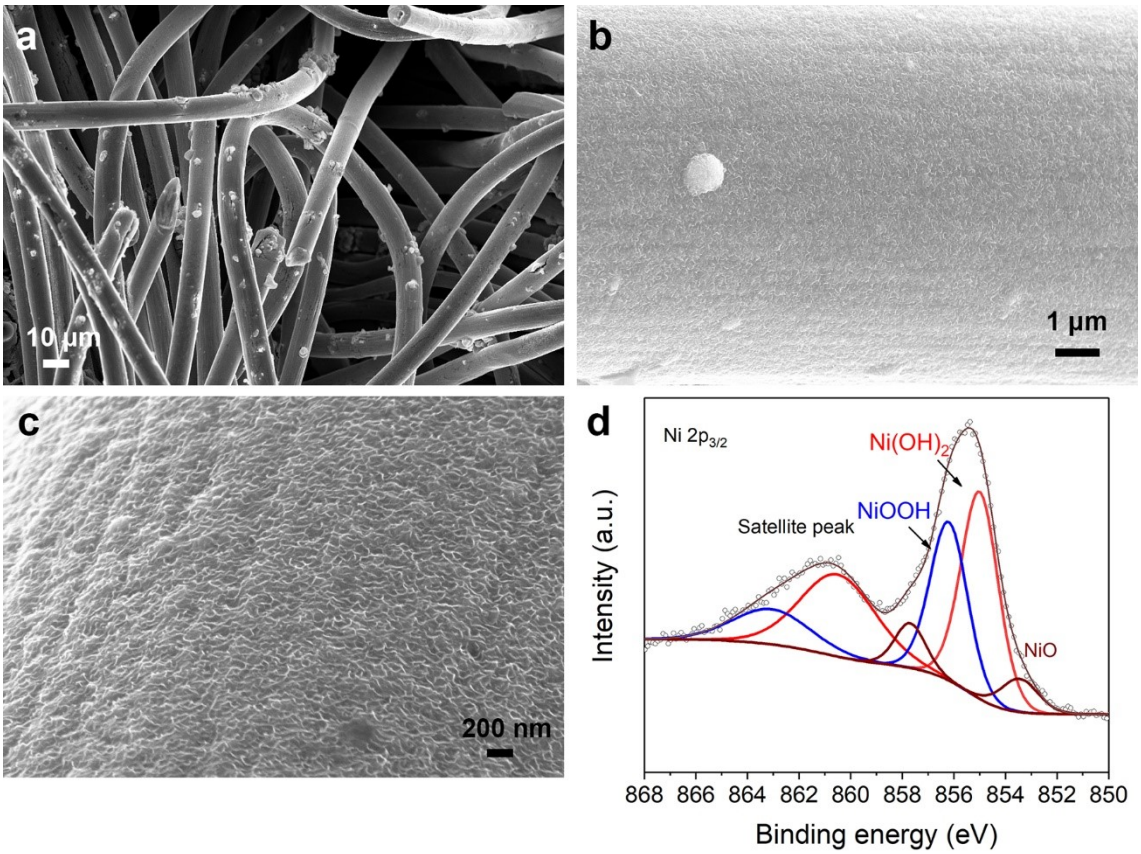

Figure S3**.** The characterization of the SVT catalyst. a)-c) SEM images of SVT catalyst on carbon cloth. d) Ni $2p_{3/2}$ XPS spectra of the SVT catalyst. Note that SVT catalyst is composed with surface nickel (oxy)-hydroxide as catalytic sites and internal metal nickel as conducting layer.

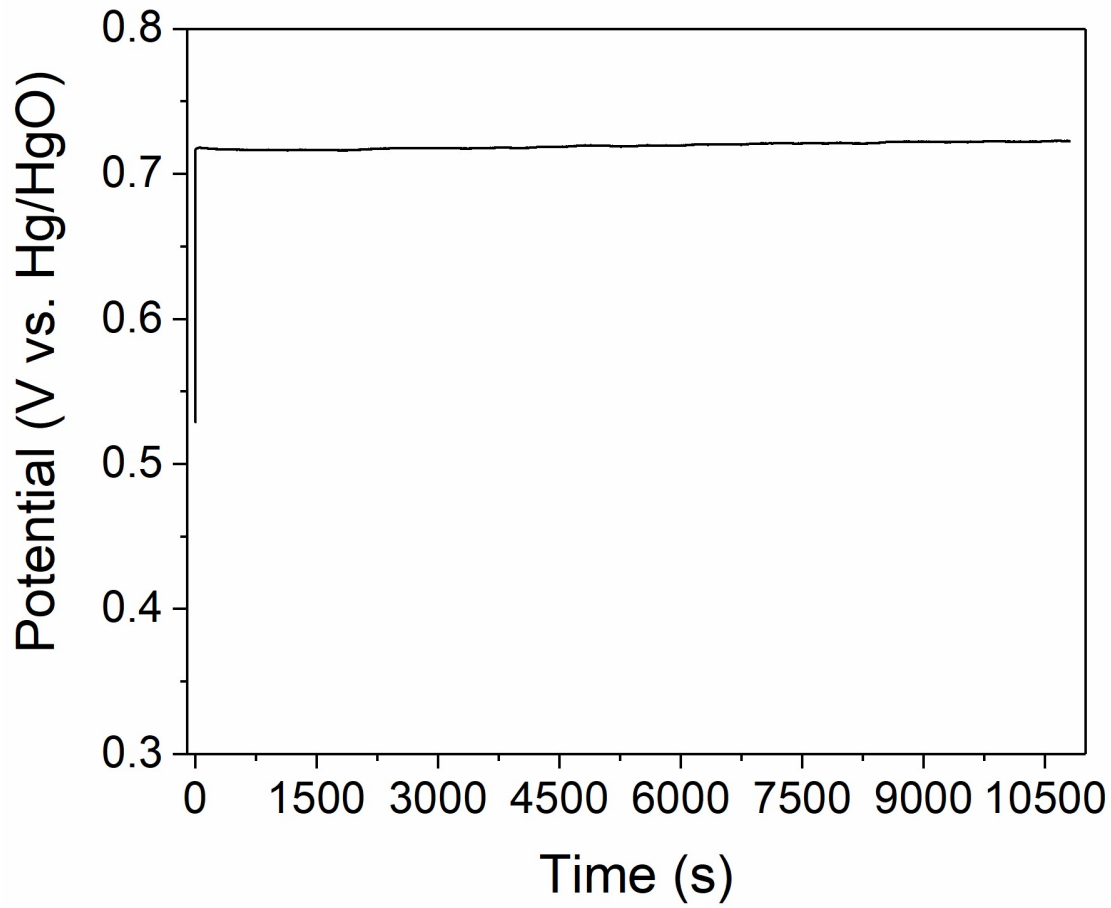

Figure S4**.** Potential of electrodeposited Ni in 1 M KOH electrolyte recorded over a long period at a current density 30 mA cm^{-2}.

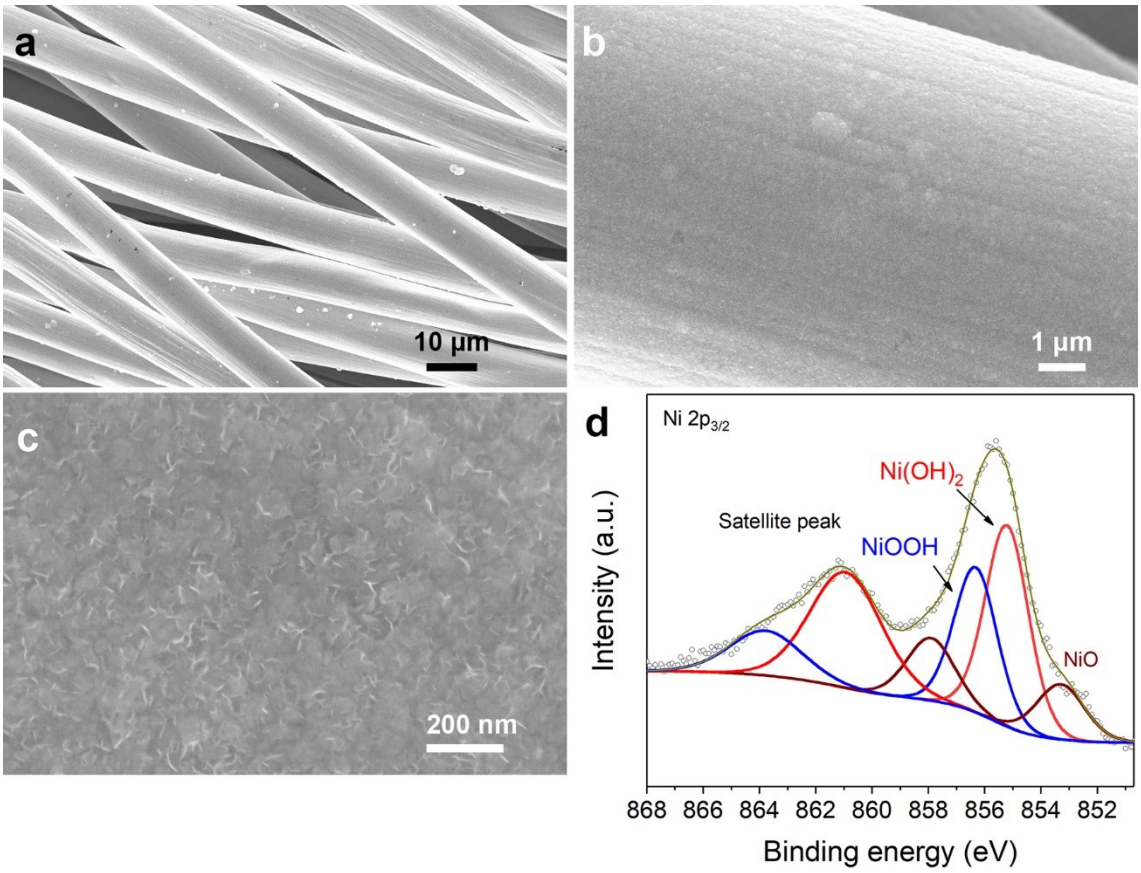

Figure S5**.** The characterization of activated Ni. a)-c), SEM images of activated Ni on carbon cloth in pure KOH electrolyte. d) Ni $2p_{3/2}$ XPS spectra for the activated Ni. Note that activated Ni is composed with surface nickel (oxy)-hydroxide and internal metal nickel as conducting layer.

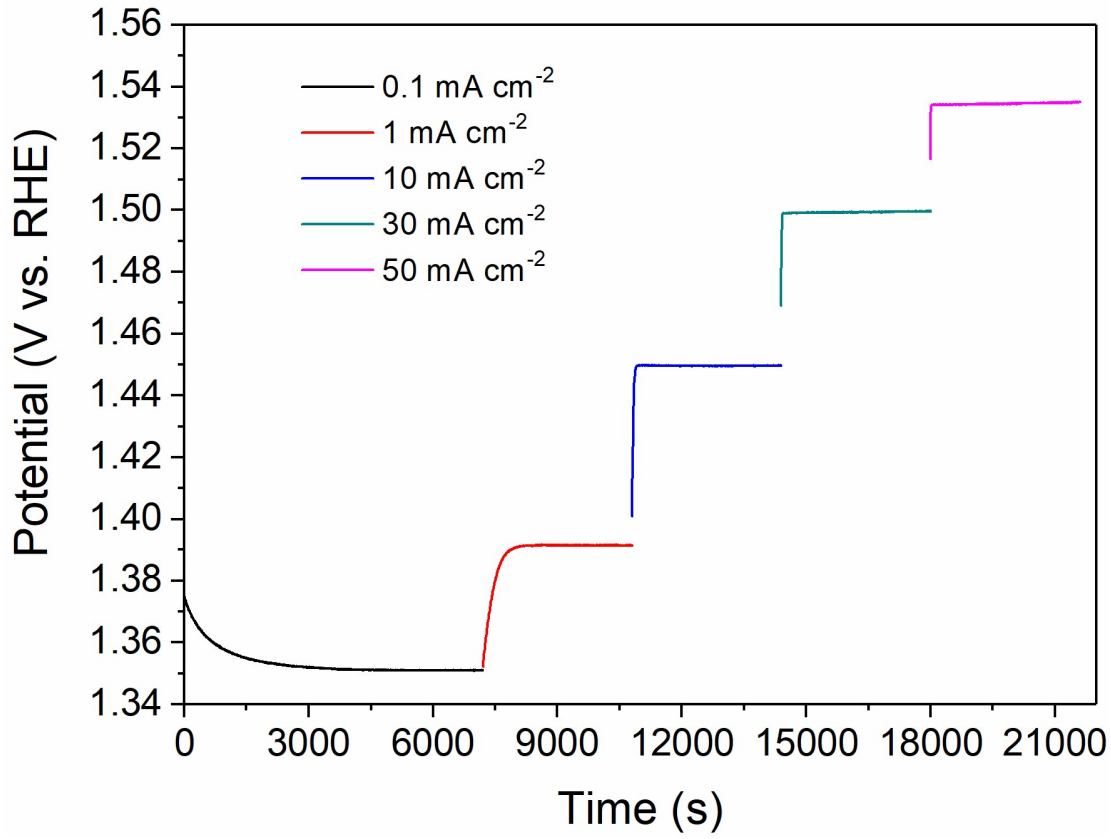

Figure S6. Time dependence of recorded potential during electrolysis using SVT catalyst for different current densities from 0.1 to 50 mA cm^{-2}.

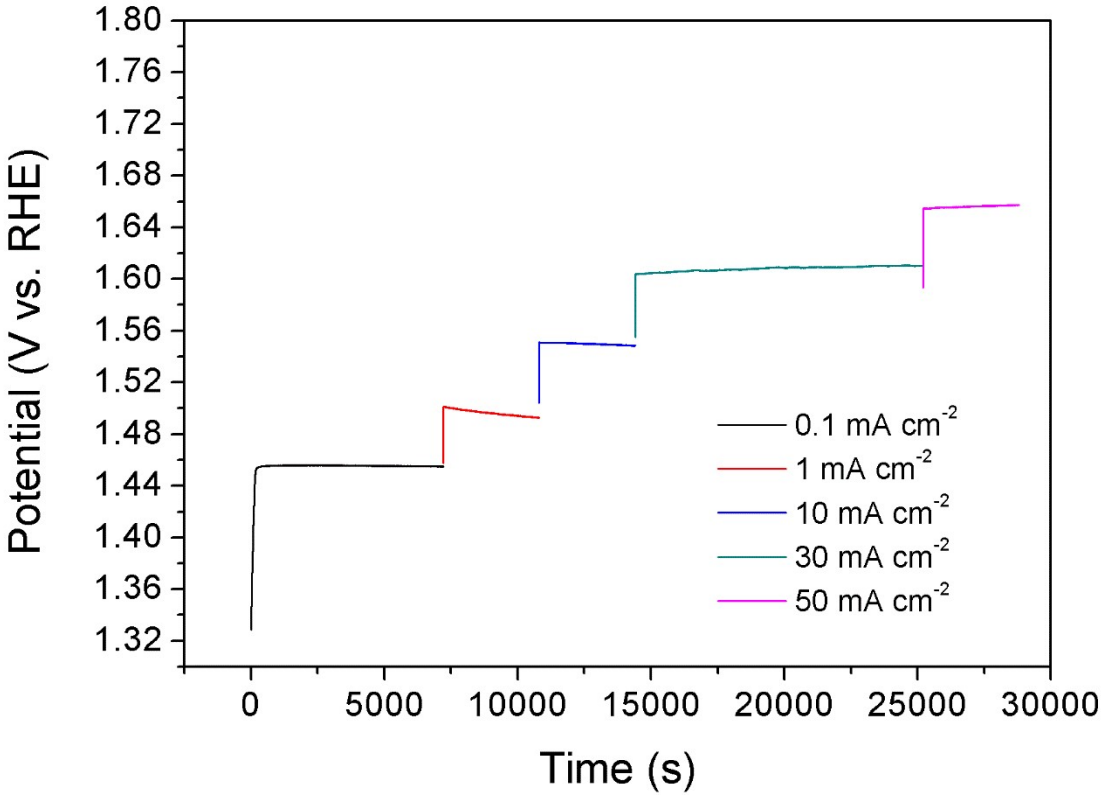

Figure S7. Time dependence of recorded potential during electrolysis using activated Ni catalyst for different current densities from 0.1 to 50 mA cm^{-2}.

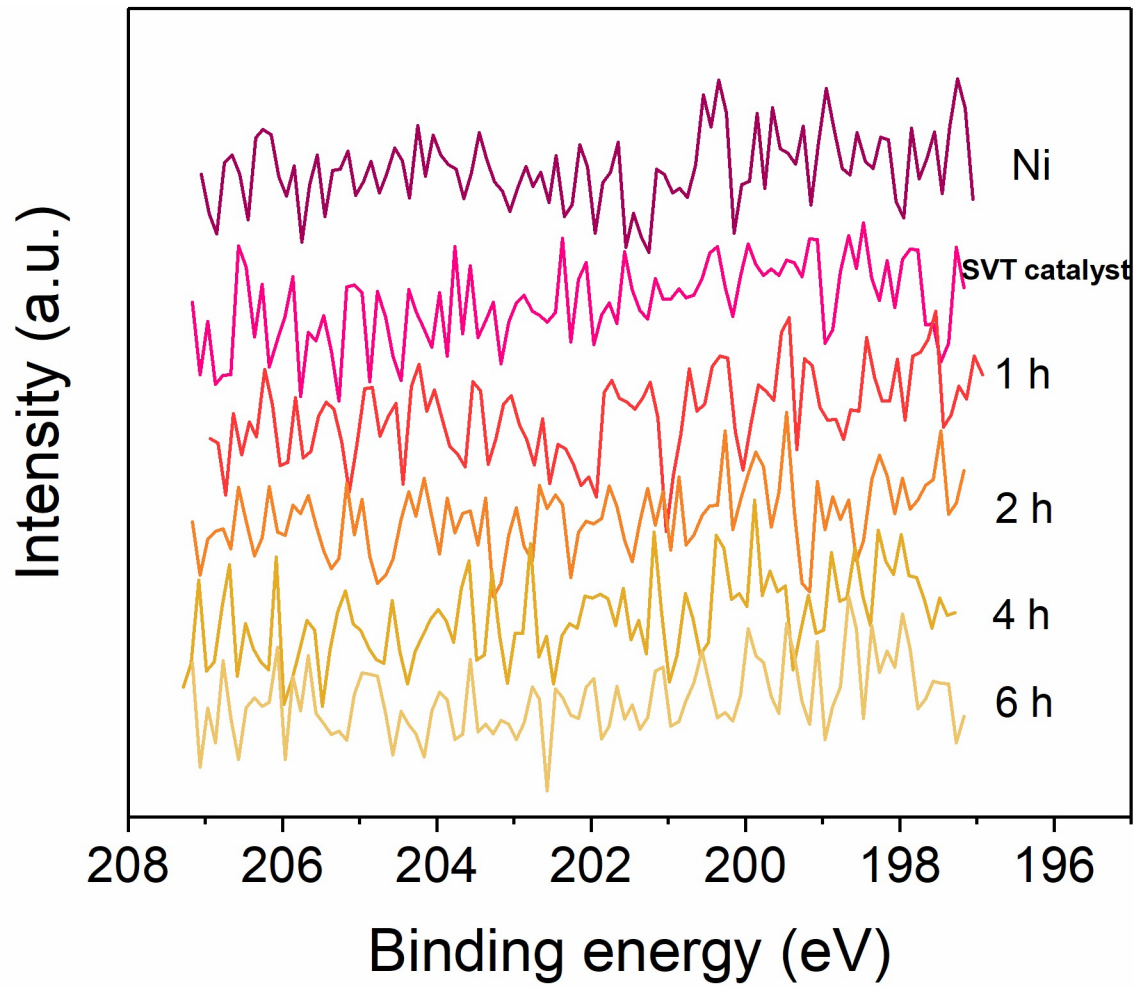

Figure S8. Cl 2p XPS spectra of electrodeposited Ni, SVT catalyst, and SVT catalyst after operating for different time (i.e., 1, 2, 4, 6 hours; corresponding to the bottom four spectra).

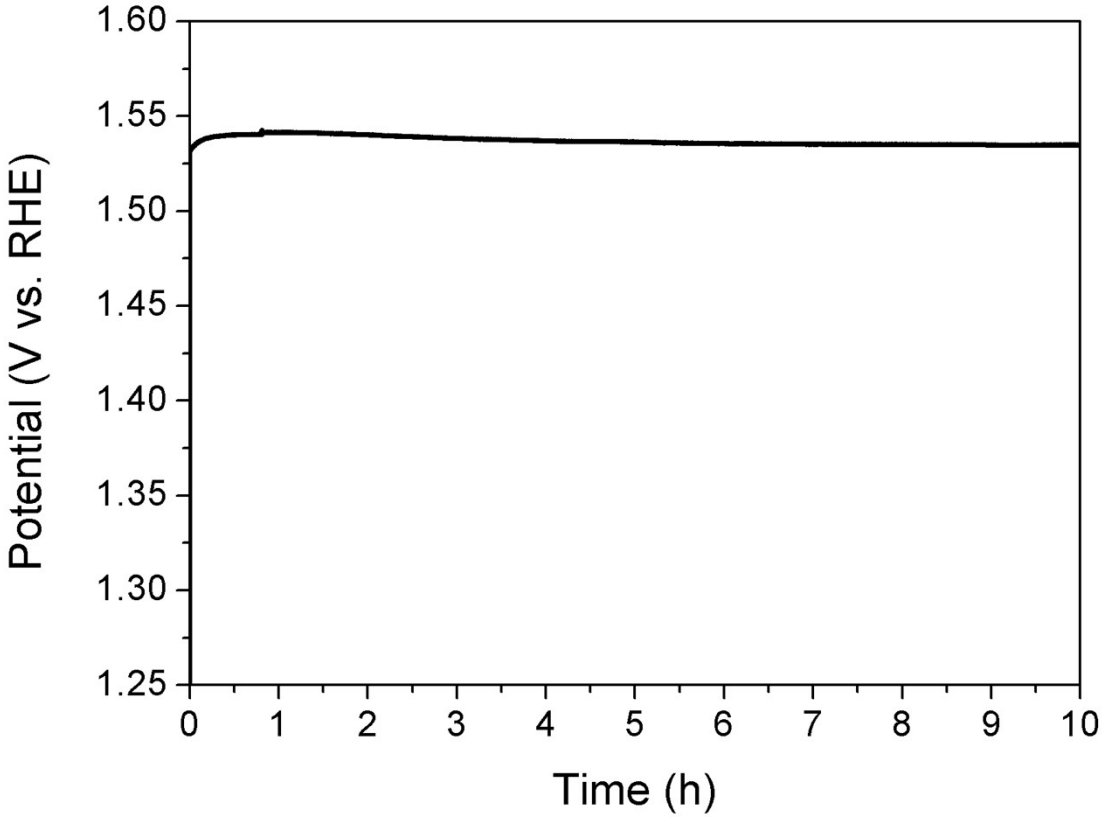

Figure S9**.** Time dependence of recorded potential during electrolysis involving activated Ni catalyst at a current density of 10 mA cm^{-2}.

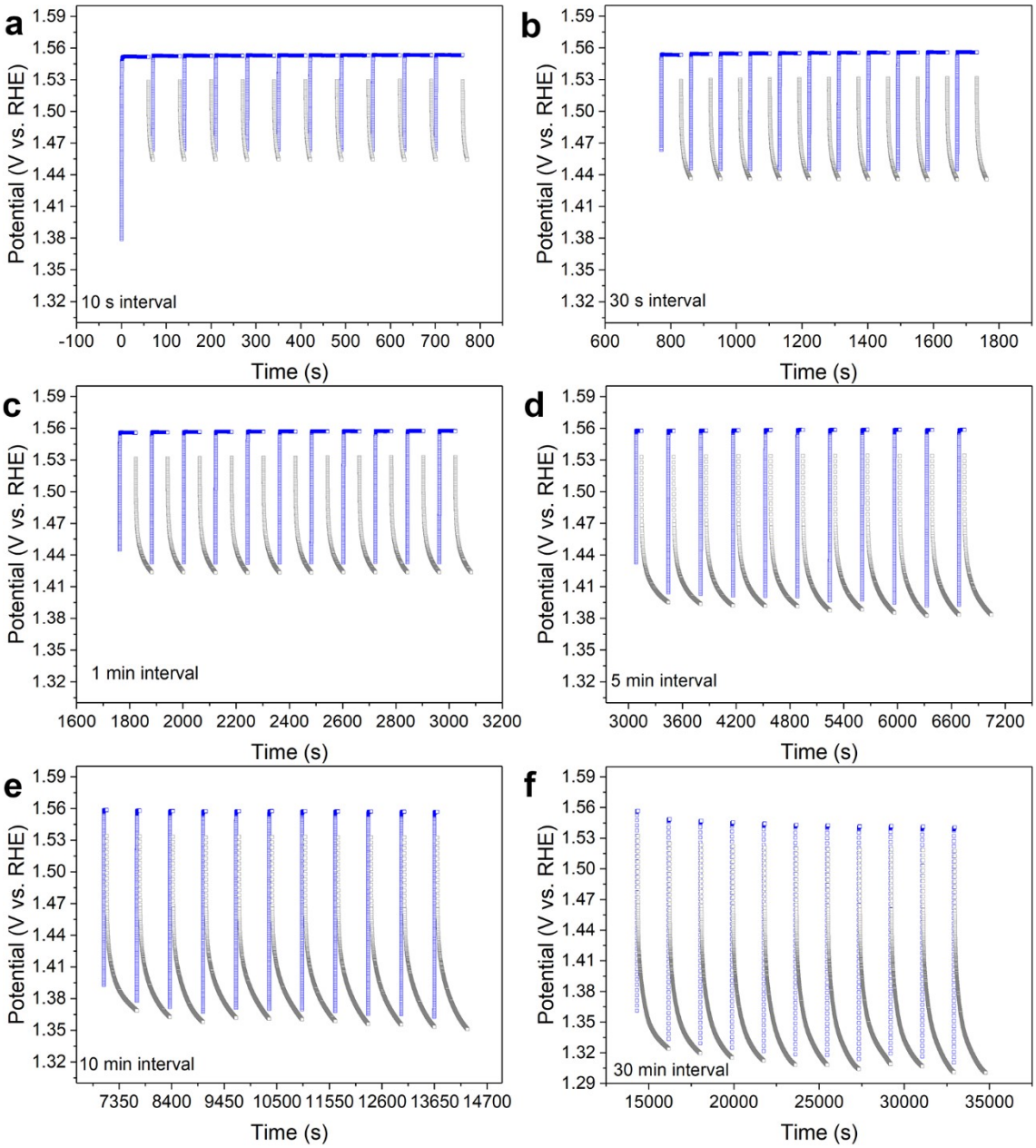

Figure S10**.** Electrocatalytic performance of the activated Ni catalyst under IEM operation. a)-f) Potential measured during cycling of the activated Ni catalyst between a 1-min power-on time (at 10 mA cm^{-2}) and different power-off times of 10 s (a), 30 s (b), 1 min (c), 5 min (d), 10 min (e), 30 min (f) (i.e., the IEM of operation). Blue dotted line and grey dotted line represent potential recorded during power-on and power-off, respectively.

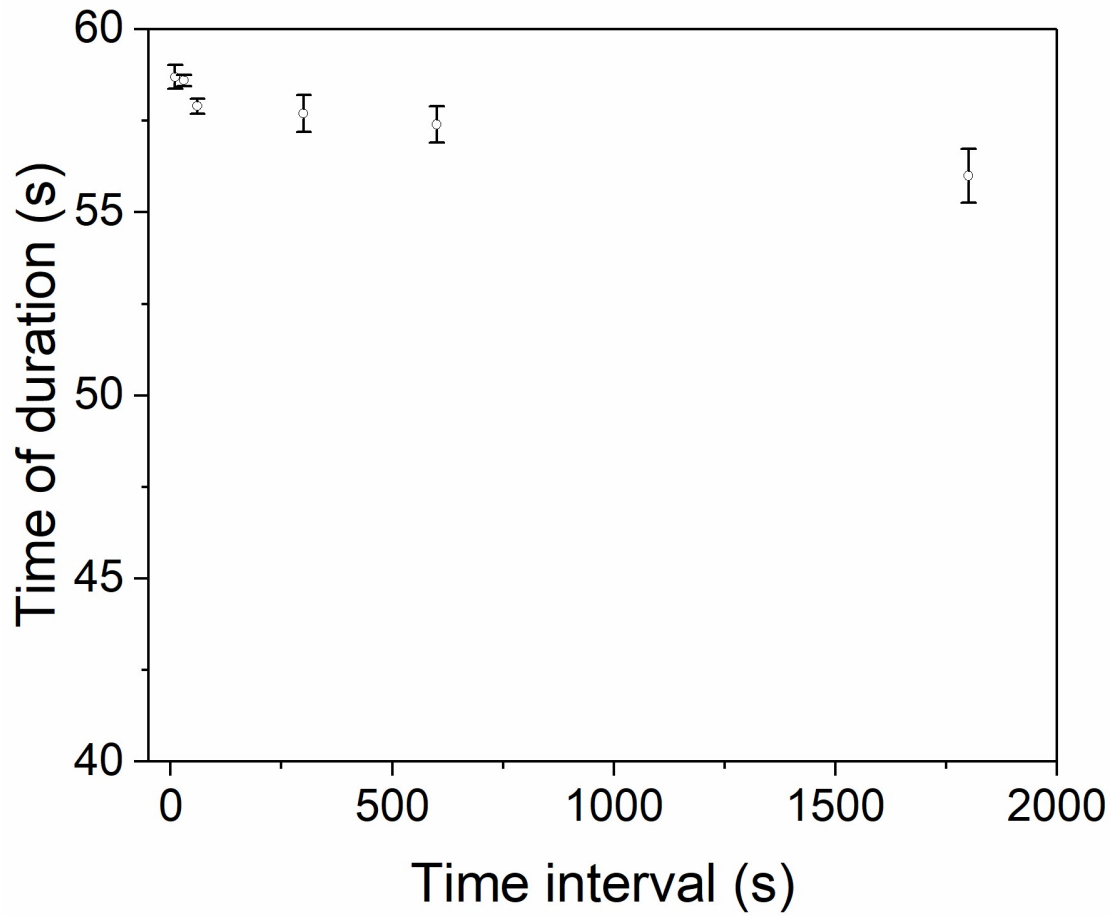

Figure S11**.** Time at which the potential becomes stable at the current density of 10 mA cm^{-2} during the IEM operation of the activated Ni catalyst, as a function of the power-off interval. This time refers to the instant when the potential stops changing after application of the oxidation current in Figure S11.

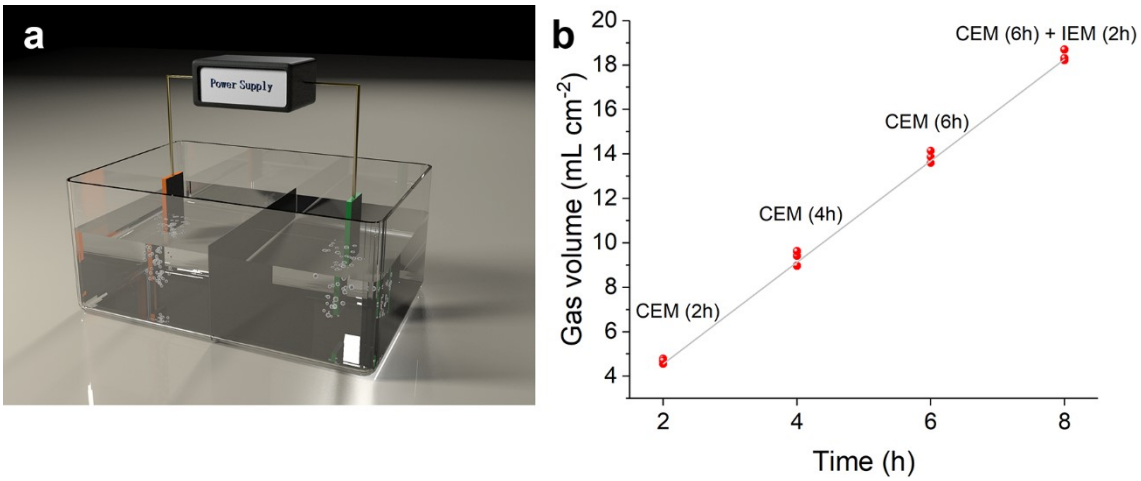

Figure S12**.** The Faradic efficiency for the SVT catalyst under CEM and IEM operation. a) Schematic representation of a two-electrode electrocatalytic cell with an anion-exchange membrane for collecting the gas generated. SVT catalyst and graphite paper serve as the working electrode and counter electrode, respectively. b) Experimentally collected gas volume after deducting hydrogen (red circles) and theoretically calculated gas volume (grey line, indicating 100% Faradaic efficiency) as a function of time for which a current density of 10 mA cm^{-2} was applied. The gas generated was collected every 2 hours for both continuous and intermittent electrocatalytic modes of operation, denoted as CEM and IEM, respectively. For the latter, the power-on time was 1 min and power-off time was 5 min. All data were collected at around 25 °C.

Table S1. OER overpotentials of different monometal nickel-based catalysts at the current density of 10 mA cm^{-2}.

Catalysts/ precursors	Overpotential at 10 mA cm^{-2}	Catalytic mode	Interval time of IEM	Ref.
SVT catalyst	215 ± 12 mV	IEM	10 s	Our work
SVT catalyst	209 ± 2 mV	IEM	1 min	Our work
SVT catalyst	189 ± 6 mV	IEM	5 min	Our work
SVT catalyst	178 ± 3 mV	IEM	10 min	Our work
SVT catalyst	165 ± 5 mV	IEM	30 min	Our work
SVT catalyst	230 mV*	CEM		Our work
Ordered mesoporous Ni sphere arrays	254 mV	CEM		10
Ni_3Se_2	290 mV	CEM		11
α-$Ni(OH)_2$	331 mV	CEM		12
β-$Ni(OH)_2$	444 mV	CEM		12
Ni_2P	290 mV	CEM		13
Ni_3S_2	217 mV	CEM		14
3D NiO_x/Ni	390 mV	CEM		15
NiO	430 mV	CEM		16
Ni_3N	233 mV	CEM		17
$NiPS_3$	360 mV	CEM		18

* average overpotential calculated based on long-term constant current oxidation.
CEM and IEM represent continuous and intermittent electrocatalytic modes of operation, respectively.

Movie S1. The bubble generation in electrolyte for the SVT catalyst at 1.35 V vs. RHE.

Movie S2. The bubble generation in electrolyte for the SVT catalyst at 1.45 V vs. RHE.

Movie S3. The bubble generation in electrolyte during power-on (at the current density of 30 mA cm^{-2}) and power-off period for the SVT catalyst.

Movie S4. The bubble generation of side view of electrode in electrolyte during power-off period for the SVT catalyst taken out and remove surface electrolyte (power-on period: the current density of 30 mA cm^{-2}).

Movie S5. The bubble generation of front view of electrode in electrolyte during power-off period for the SVT catalyst taken out and remove surface electrolyte (power-on period: the current density of 30 mA cm^{-2}).

Reference

[1] Y. Du, Y. Zhu, S. Xi, P. Yang, H. O. Moser, M. B. H. Breese, A. Borgna, *J. Synchrotron Radiat.* **2015**, *22*, 839-843.

[2] B. Zhou, L. Guo, Y. Zhang, J. Wang, L. Ma, W. Zhang, Z. Fu, Z. Peng, *Adv. Mater.* **2017**, *29,* 1701568.

[3] S. Ma, Y. Wu, J. Wang, Y. Zhang, Y. Zhang, X. Yan, Y. Wei, P. Liu, J. Wang, K. Jiang, S. Fan, Y. Xu, Z. Peng, *Nano Lett.* **2015**, *15*, 8084-8090.

[4] D. Vanderbilt, *Phys Rev B Condens Matter* **1990**, 41, 7892–7895.

[5] P. Giannozzi, S. Baroni, N. Bonini, M. Calandra, R. Car, C. Cavazzoni, D. Ceresoli, G. L. Chiarotti, M. Cococcioni, I. Dabo, A. D. Corso, S. d. Gironcoli, S. Fabris, G. Fratesi, R. Gebauer, U. Gerstmann, C. Gougoussis, A. Jokalj, M. Lazzeri, L. Martin-Samos, N. Marzari, F. Mauri, R. Mazzarello, S. Paolini, A. Pasquarello, L. Paulatto, C. Sbraccia, S. Scandolo, G. Sclauzero, A. P. Seitsonen, A. Smogunov, P. Umari, R. M. Wentzcovitch, *J Phys Condens Matter* **2009**, 21, 395502.

[6] B. Hammer, L. B. Hansen, J. K. Nørskov, *Phys. Rev. B* **1999**, 59, 7413–7421.

[7] M. Cococcioni, S. d. Gironcoli, Phys. Rev. B **2005**, 71, 035105.

[8] D. Friebel, M. W. Louie, M. Bajdich, K. E. Sanwald, Y. Cai, A. M. Wise, M. Cheng, D. Sokaras, T. Weng, R. Alonso-Mori, R. C. Davis, J. R. Bargar, J. K. Nørskov, A. Nilsson, A. T. Bell, *J. Am. Chem. Soc.* 2015, 137, 1305–1313.

[9] J. K. Nørskov, J. Rossmeisl, A. Logadottir, L. Lindqvist, *J. Phys. Chem. B* **2004**, 108, 17886–17892.

[10] T. Sun, L. Xu, Y. Yan, A. A. Zakhidov, R. H. Baughman, J. Chen, *ACS Catal.* **2016**, *6*, 1446-1450.

[11] A. T. Swesi, J. Masud, M. Nath, *Energy Environ. Sci.* **2016**, *9*, 1771-1782.

[12] M. Gao, W. Sheng, Z. Zhuang, Q. Fang, S. Gu, J. Jiang, Y. Yan, *J. Am. Chem. Soc.* **2014**, *136*, 7077-7084.

[13] L. Stern, L. Feng, F. Song, X. Hu, *Energy Environ. Sci.* **2015**, *8*, 2347-2351.

[14] C. Ouyang, X. Wang, C. Wang, X. Zhang, J. Wu, Z. Ma, S. Dou, S. Wang, *Electrochim. Acta* **2015**, *174*, 297-301.

[15] G. Han, Y. Liu, W. Hu, B. Dong, X. Li, X. Shang, Y. Chai, Y. Liu, C. Liu, *Appl. Surf. Sci.* **2015**, *359*, 172-176.

[16] X. Yu, Y. Feng, B. Guan, X. W. Lou, U. Paik, *Energy Environ. Sci.* **2016**, *9*, 1246-1250.

[17] X. Wang, Q. Li, P. Shi, J. Fan, Y. Min, Q. Xu, *Small* **2019**, *15*, 1901530.

[18] B. Konkena, J. Masa, A. J. R. Botz, I. Sinev, W. Xia, J. Koβmann, R. Drautz, M. Muhler, W. Schuhmann, *ACS Catal.* **2017**, *7*, 229-237.